Microstructural evolution of cryomilled Ti/Al mixture during high-pressure torsion

Hamed Bahmanpour,[a] Yu Sun, Tao Hu, and Dalong Zhang
Department of Chemical Engineering and Materials Science, University of California, Davis, California 95616

Jittraporn Wongsa-Ngam
Department of Mechanical Engineering, Faculty of Engineering, King Mongkut's Institute of Technology Ladkrabang, Bangkok 10520, Thailand

Terence G. Langdon
Departments of Aerospace and Mechanical Engineering and Materials Science, University of Southern California, Los Angeles, California 90089-1453; and Materials Research Group, Faculty of Engineering and the Environment, University of Southampton, Southampton SO17 1BJ, United Kingdom

Enrique J. Lavernia
Department of Chemical Engineering and Materials Science, University of California, Davis, California 95616

(Received 29 August 2013; accepted 30 December 2013)

To provide insight into the influence of the length scale on the kinetics of phase evolution during severe plastic deformation, we studied the microstructure evolution of cryomilled Al and Ti mixture, which is further subjected to high-pressure torsion (HPT). The cryomilled microstructure consisted of elemental Al and Ti, and the subsequent HPT deformation at ambient temperature led to the solid state formation of Al-rich intermetallics. X-ray diffraction peaks originating from $TiAl_2$ and $TiAl_3$ were observed after one revolution of HPT, suggesting a shear strain-assisted formation of the intermetallics. A high resolution transmission electron microscope confirmed the formation of $TiAl_2$ following HPT for one revolution. Further HPT straining led to microstructure refinement and a mixing of the Ti and Al, as well as of any phases formed initially. The solid state formation of the intermetallics and the overall evolution of the microstructure are discussed based on the generation of a high density of lattice defects that evolve under the strain conditions present during HPT.

I. INTRODUCTION

Severe plastic deformation (SPD) routes, such as high energy ball milling,[1] high-pressure torsion (HPT),[2] and equal channel angular pressing (ECAP),[3,4] have been used in research related to intermetallic compounds that are generally hard and brittle at room temperature. The formation of intermetallics typically involves elevated temperature processing due to slow diffusion in these ordered structures. Therefore, attempts have been focused on increasing the processing temperature to facilitate the diffusion of atomic species in the microstructure. For example, it is reported that HPT at an elevated temperature leads to the formation of Al_3Ni_2 in the Ni–Al system[5] and $TiAl_3$, $TiAl_2$, and TiAl in the Ti–Al system.[6] In this respect, combined SPD techniques were proven to provide interesting and unique microstructures due to the different deformation paths involved in each process. In related studies, a combination of ECAP + rolling[7] and ECAP + HPT[8] was utilized in an effort to tailor the microstructures of Cu–30%Zn and of Cu–0.1%Zr alloys, respectively. Furthermore, ball milling + ECAP and ball milling + HPT were utilized for Ti–Al[9] and Cu–30%Zn[10] systems, respectively, for the purpose of consolidation and producing bulk nanostructured alloys with enhanced mechanical properties.

In the case of coarse-grained diffusion couples such as Al–Cu, it has been shown that the applied shear strain during HPT contributes significantly to the formation of lattice defects that elevate the diffusion rate of atoms by a factor of 10^{12}–10^{22}.[11] In this regard, the solid state formation of intermetallic compounds has been reported in elevated temperature processing of a coarse-grained Al and Ti mixture.[6] The resultant microstructure is composed of a bimodal grain size distribution and nanotwins that reportedly exhibit an ultrahigh yield strength of ~2.9 GPa, and a high compressive strain to failure of ~14%.

In light of the above findings, we report a study of the microstructure evolution in nanostructured Al and Ti elemental powders (prepared via cryomilling) and subjected to HPT. In particular, the goal of this study is to evaluate the influence of the high density of defects introduced during cryomilling on the resulting solid state reactions that occur between the Ti and Al during the HPT deformation.

[a]Address all correspondence to this author.
e-mail: hbahman@ucdavis.edu
DOI: 10.1557/jmr.2014.18

 © Materials Research Society 2014

https://doi.org/10.1557/jmr.2014.18 Published online by Cambridge University Press

II. EXPERIMENTAL PROCEDURE

The pure Al and Ti powders used in this study were obtained from Advanced Specialty Metals (Nashua, NH) and Valimet (Stockton, CA), respectively. The two elemental powders were blended, Ti–47 at%Al, and cryomilled for 10 h in a liquid argon environment (−181 ± 5 °C) using a modified 1-S Szegvari attritor with a stainless steel impeller (at 180 rpm; Akron, OH) and stainless steel balls (Ø6.4 mm). The mean grain sizes of the Al and Ti particles after cryomilling were 42 and 100 nm, respectively, as measured by a transmission electron microscope (TEM). Disks of 10-mm diameter were prepared by HPT processing of the cryomilled mixture under quasi-constrained conditions[12,13] with a 6.0 GPa pressure, rotation speed of 1 rpm, and revolution of 1, 5, and 10, which corresponds to equivalent shear strains at the edges of the disks, γ, of about 22, 98, and 250, respectively. The phases present in the samples were characterized, and the dislocation density was estimated using x-ray diffraction (XRD) with Cu K_α radiation. The average crystallite size and microstrain were calculated from diffraction line broadening of three major peaks of the Al and Ti using the Scherer and Wilson equation[14,15];

$$B = \frac{4K\lambda}{3D \cdot \cos\theta} + 4\varepsilon \cdot \tan\theta \quad ,$$

where K is the shape factor, λ denotes the x-ray wave length, D the crystallite size, θ the diffraction angle, and ε the microstrain. The dislocation density was also estimated using the following equation[16];

$$\rho = \frac{2\sqrt{3}(\varepsilon^2)^{1/2}}{D \cdot b} \quad ,$$

where b is the Burgers vector.

TEM samples were prepared from areas close to the edges of the HPT disks by mechanical polishing and final thinning and perforation was performed by ion milling. Microstructure studies were performed by a Philips CM-12 TEM operated at 120 kV and a JEOL 2500 high resolution transmission electron microscope (HRTEM; Eindhoven, Netherlands) operated at 200 kV.

III. RESULTS

The microstructure evolution studied by TEM shows a change in grain size at different stages of processing imposed by cryomilling and subsequent HPT. Figure 1 shows bright field TEM images from the cryomilled and HPT deformed samples. The 10 h cryomilled sample, Fig. 1(a), shows an average grain size of 42 and 100 nm for Al and Ti, respectively. The microstructure after 1 revolution of HPT (γ = 22) consists of large areas of Al and Ti that are not well mixed as shown in Fig. 1(b). The Ti phase with large grains and the Al phase with small grains can be identified clearly in the TEM images, and there is a distinct boundary between the two phases as highlighted by the dashed line. Further increase in HPT strain up to 5 revolutions (γ = 98) led to a mixing of the present phases as delineated in Fig. 1(c) and eventually, after 10 revolutions of HPT (γ = 250), produced a well-mixed microstructure of Ti, Al, and intermetallic phases as shown in Fig. 1(d). The Al and Ti grains could not be easily distinguished in the mixed microstructure of the sample with an HPT strain of 250. The deformation path is shown by a wavy microstructure highlighted by the dashed line.

Grain size measurements by TEM and the crystallite sizes estimated by XRD technique are listed in Table I. The grain size of both the Al and Ti (Table I) is essentially in the same range as suggested by the TEM studies, but the crystallite size (coherent scattering domain size) estimated by XRD for the Ti shows an increase of up to γ = 98, i.e., 36.7 nm and decreases upon further application of HPT strain. In contrast, the crystallite size for the Al phase shows a consistent increasing trend that is accompanied by a decrease in the dislocation density, and this is discussed in the section that follows.

XRD was also utilized to further investigate the microstructure and phase evolution in Fig. 2. The XRD profile of the cryomilled mixture shows the elemental Ti and Al peaks. When shear strain is applied to the cryomilled powder so that γ = 22, it is evident that the XRD peak heights are slightly increased and, interestingly, new peaks are also present in this sample. These new peaks correspond to the Al-rich intermetallic phases of $TiAl_3$ and $TiAl_2$. Further applications of shear strain by HPT to γ = 98 and γ = 250 appear to contribute mostly to microstructure refinement rather than any evolution of new phases, as determined by substantial broadening of the peaks due to the small crystallite size and high density of the lattice defects. Progressive broadening of the low angle peaks and simultaneous vanishing of the high angle peaks can be seen for the samples deformed up to γ = 98 and γ = 250. It should be noted that the applied strain also causes the intermetallic phases to deform and, possibly due to their small quantity, their broadened peak cannot be resolved by XRD. Furthermore, the peak shift of Ti $(10\bar{1}1)$ shows the insertion of the Al atoms in the Ti lattice as a substitutional alloying element. These results suggest that there is a solid state promotion of intermetallic formation in the Ti–Al system upon application of the HPT strain, and this is discussed in more detail in the discussion that follows.

Careful examination of the XRD profiles revealed the dislocation density evolution in the hcp Ti and fcc Al during the cryomilling and HPT processing as documented in Fig. 3. It is seen that the cryogenic processing

https://doi.org/10.1557/jmr.2014.18 Published online by Cambridge University Press

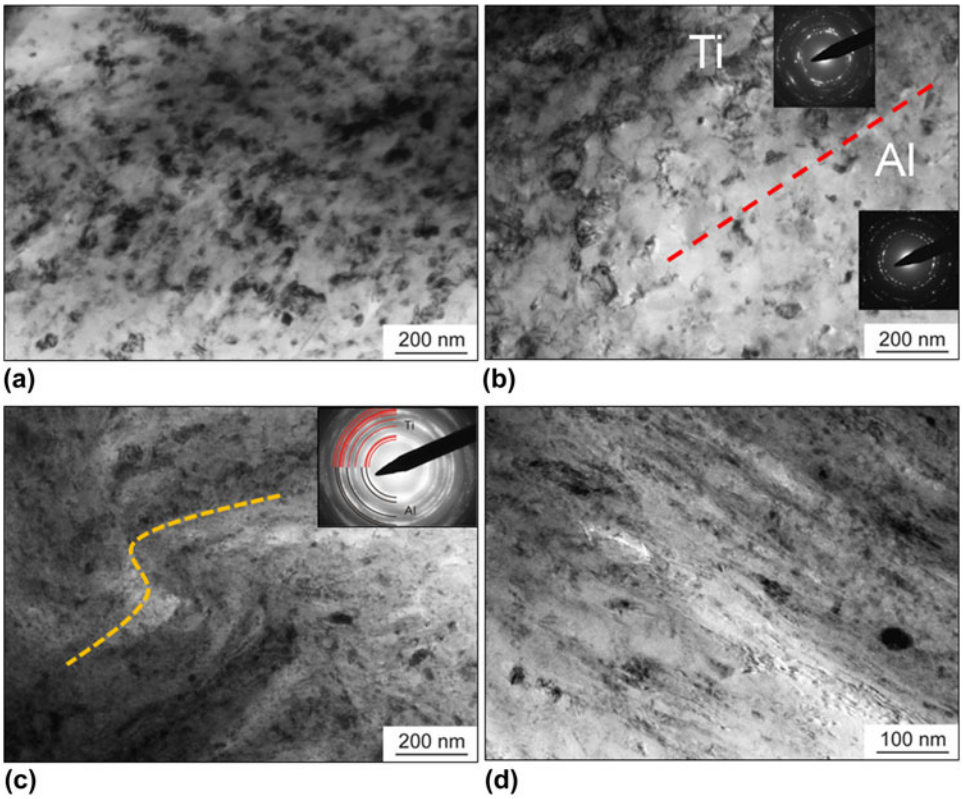


FIG. 1. TEM images of the 10-h cryomilled powder (a) and subsequently deformed by HPT to (b) $\gamma = 22$, (c) $\gamma = 98$, and (d) $\gamma = 250$. Insets in (b) show selected area diffraction pattern of hcp Ti and fcc Al phases that are not mixed very well. SAED in (c) shows mixed microstructure consisted of Ti and Al phases.

TABLE I. Grain and crystallite size of Ti and Al measured by TEM and XRD, respectively.

	Grain size (nm)			
	Ti		Al	
	XRD	TEM	XRD	TEM
10 h cryomilled	26.0	100 ± 34	23	42 ± 18
10 h cryomilled + HPT ($\gamma = 22$)	35.9	86 ± 30	44	58 ± 30
10 h cryomilled + HPT ($\gamma = 98$)	36.7	68 ± 19	49	38 ± 16
10 h cryomilled + HPT ($\gamma = 250$)[a]	22.8	...	67	...

[a]Ti and Al phases are not easily distinguishable by TEM in this sample.

of the elemental blend of Ti and Al resulted in defect accumulation and hence a high dislocation density in the cryomilled powder. Further processing by HPT at room temperature leads to a progressive decrease in dislocation density for the Al. However, the Ti shows similar behavior up to a shear strain of 98, but the application of further shear strain, $\gamma = 250$, elevates the dislocation density so that it is even higher than the initial dislocation density in the cryomilled mixture.

As revealed by the XRD results in Fig. 2, the formation of the intermetallic phases occurs at an HPT strain of 22. More detailed TEM studies were performed on the HPT disk subjected to $\gamma = 22$ to obtain a better understanding of the microstructure and present phases. A diffraction pattern taken from the area in Fig. 4(a) has diffraction spots near the center of the pattern that are related to the intermetallic phases. A representative dark field image is shown in Fig. 4(c), which was taken using the diffraction spot shown in Fig. 4(b). It is seen that the fine nanosized intermetallic phases are uniformly dispersed in the matrix. An HRTEM image from one of the intermetallic particles is shown in Fig. 4(d), and the fast Fourier transform (FFT) pattern in the inset shows characteristic crystallographic planes corresponding to the tetragonal $TiAl_2$ intermetallic in the Ti–Al system.

IV. DISCUSSION

Cryogenic plastic deformation is known to minimize the dynamic recovery of lattice defects, such as dislocations and vacancies, and hence leads to the formation of a fine-grained microstructure with a high density of defects.[17,18] The mechanism of microstructure formation during cryomilling includes a flattening of the initial powder from its original shape and an accumulation of dislocations in the microstructure upon repeated fracturing and cold welding. Earlier studies on mechanical alloying of Ti and Al mixtures proved the formation of a mixture of disordered hcp solid

https://doi.org/10.1557/jmr.2014.18 Published online by Cambridge University Press

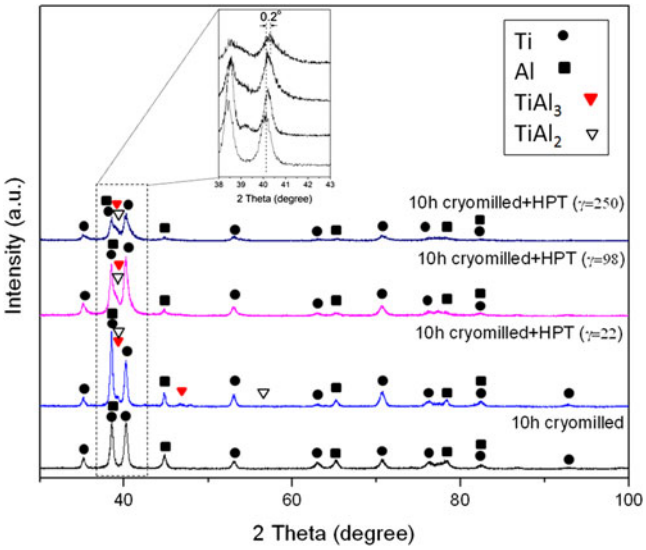


FIG. 2. XRD profiles of samples after 10 h cryomilling and subsequent HPT deformation. Inset shows peak shift for Ti$(10\bar{1}1)$.

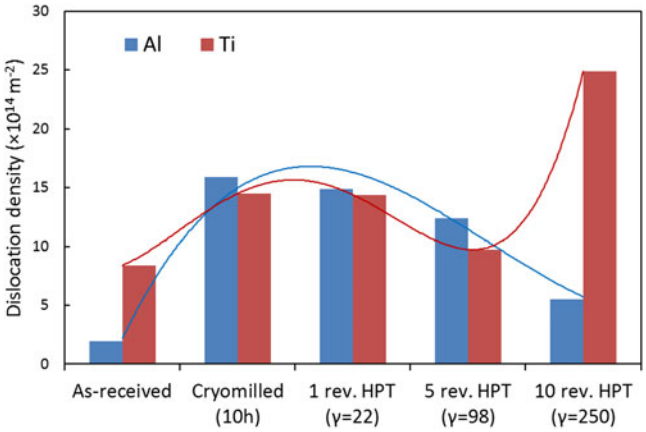


FIG. 3. Dislocation density evolution upon cryomilling and subsequent deformation by HPT in Ti and Al.

solution and amorphous phases upon extended room temperature ball milling up to 150 h.[19] High energy ball milling of Ti–48Al powder blend was also reported to result in nanocrystalline and amorphous microstructure formation.[20] In a study of the 5083 Al alloy, it was found that cryomilling can suppress crystallization due to a local temperature rise during the mechanical alloying process and leads to an amorphization of the powder. In our Ti/Al blend, 10 h milling at cryogenic temperature resulted in a breakdown of the initial microstructure to a nanostructure with grain sizes of 42 and 100 nm for the Al and Ti, respectively, as revealed by the TEM studies in Fig. 1. It is evident from the XRD profiles that the cryomilled powder only consists of a mixture of Ti and Al phases in Fig. 2. Since thermally driven dynamic recovery is effectively suppressed at a low temperature, the resultant mixture after the cryomilling has a high density of dislocations, which are accumulated in the course of the milling process ($\rho_{Ti} = 14.5 \times 10^{14}$ m^{-2} and $\rho_{Al} = 15.9 \times 10^{14}$ m^{-2}) in Fig. 3. These nanostructured powders contain a high density of defects and become the precursor for a post-cryomilling step by means of HPT.

In a study on coarse grain pure Cu and Al, it was reported that dynamic recrystallization and recovery during HPT processing can contribute to annihilation of stored dislocations in the microstructure and hence results in a decrease in dislocation density.[21] Interestingly, an application of HPT strain on electrodeposited Ni–20%Fe samples with initial grain size of 22 nm showed a decrease in dislocation density after 1 HPT revolution and an increase with further application of HPT strain up to 9 revolutions.[22] This is consistent with our observation in the Ti/Al mixture where HPT strain causes the dislocation density to decrease in the case of the Al phase and decrease and then increase in the case of the Ti phase. This change in dislocation density evolution after deformation of a nanostructure was also reported in Ni–18Fe[23] alloy subjected to rolling deformation and pure Ni[24] subjected to HPT. It is known that the HCP Ti has different mechanical responses compared with that of FCC metals due to the limited activation of slip systems at room temperature, and hence, dislocation slip is accompanied by twinning to accommodate plastic deformation. However, deformation twinning in Ti is difficult as the grain size decreases due to the lack of screw pole dislocations that could couple the two adjacent slip planes in this grain size regime.[25] Therefore, the dislocation density evolution of the nanocrystalline Ti should be comparable to the FCC Ni and Ni–Fe alloys since they are all dominated by the dislocation slip mechanism.

The mechanism of dislocation density change during SPD was discussed by Wang et al.[22] When dislocations in a nanocrystalline structure are activated by an applied stress, they are very unstable and prone to glide through the grains and disappear at the grain boundaries. This is considered to be the mechanism of dislocation density decrease for nanostructures during SPD.[22,23] As mentioned above, it is reported that the dislocation density in nanocrystalline Ni–20%Fe alloy during HPT also decreases initially and then increases.[22] The mechanism of dislocation density increase was attributed to the elimination of low angle grain boundaries during grain growth via grain rotation and the boundary dislocations that accommodate the disorientations interact and tangle with each other to hinder the motion of dislocations and provide dislocation multiplication sources. This is in agreement with our observation of dislocation density and crystallite size change in our samples. In our study, no significant grain growth was observed for the Al and Ti in the HPT processed samples as indicated by the TEM grain size analysis in Table I. However, the crystallite size data estimated by XRD in Table I provide a clear insight into the competitive evolution of dislocation density in the

https://doi.org/10.1557/jmr.2014.18 Published online by Cambridge University Press

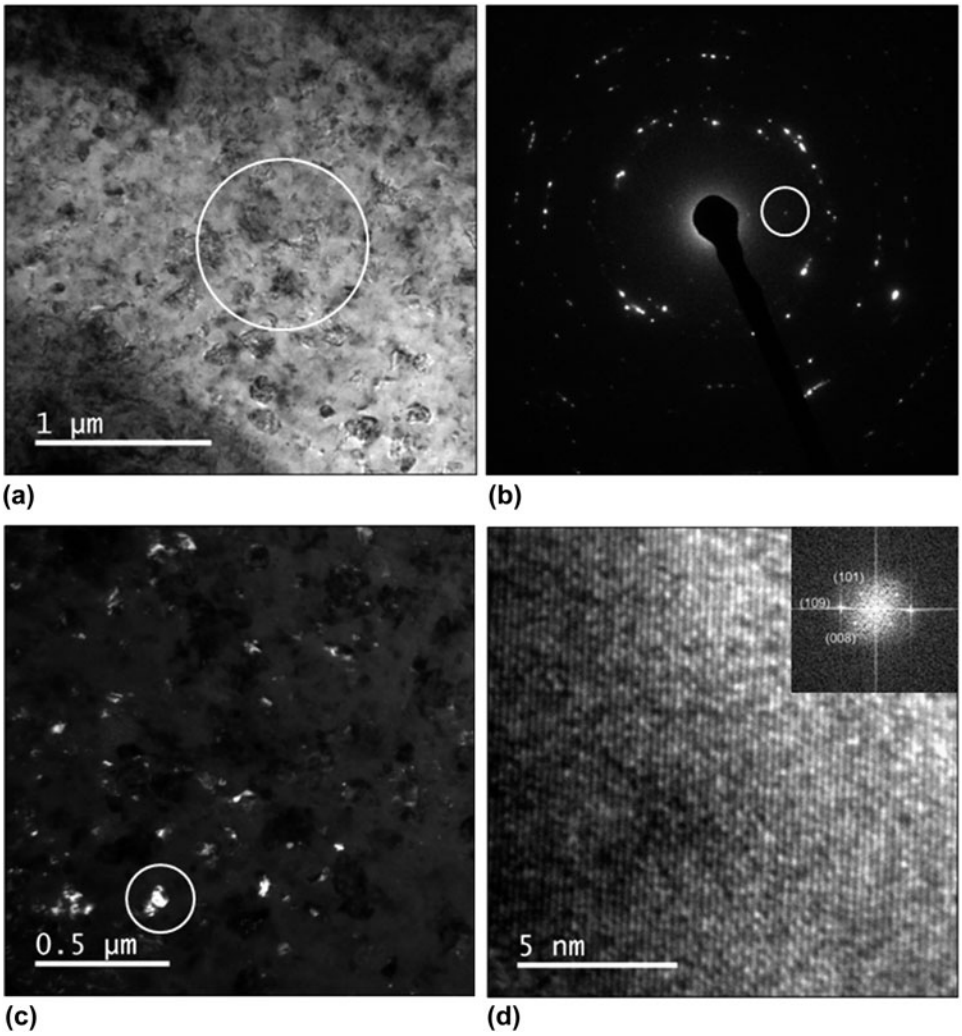


FIG. 4. (a) Bright field TEM image of the sample subjected to HPT strain of 22. (b) SAD pattern of the area shown in (a). (c) Dark field TEM image using diffraction spot shown by a circle in (b). (d) HRTEM image of an intermetallic particle shown by a circle in (c). Inset shows FFT pattern showing the tetragonal crystal structure of $TiAl_2$.

Al and Ti. Increased HPT strain leads to dynamic recovery of dislocations that is reflected as an increase of crystallite size and a decrease of the dislocation density in Al up to $\gamma = 250$ and in Ti up to $\gamma = 98$. It appears that an HPT strain of more than $\gamma = 98$ leads to a further storage of dislocations in Ti that is also accompanied by a decrease of crystallite size to 22.8 nm. This indicates that elimination of low angle grain boundaries should also play a role in our system, and boundary dislocations interact and tangle with each other to enhance dislocation density.

Unlike the Ni–Fe system that has a wide solubility limit and is expected to be chemically stable, there is a high diffusion flux from the Al to Ti during HPT processing. Due to the zero equilibrium solubility of Ti in Al and about 11% solid state solubility of Al in Ti at room temperature,[26] Al deformed statically as a pure metal and Ti deformed dynamically by alloying with Al. As is evident from the XRD profiles, the $(10\bar{1}1)$ peak of Ti shifts to a high angle and no peak shift was observed for Al after HPT processing. While Al atoms diffuse into the Ti lattice, vacancies, dislocations, and grain boundaries are the diffusion paths, and the solute Al atoms can reduce the dislocation formation energy when they segregate to the dislocation core[27] and perturb the dislocation mobility by a condensed solute cloud and much more diffuse solute (Cottrell) atmosphere.[28] A dynamic interaction of diffusive solute atoms with moving dislocations was studied by phase field models. It was shown that, depending on the solute diffusion mobility, doubling the solute concentration in a binary system can retard the dislocation velocity by one-half.[29] Therefore, it appears that during the initial stage of the HPT, where the Al concentration in the Ti lattice is low, dislocations in Ti are not effectively pinned by Al atoms, and hence dislocations can move rapidly and possibly annihilate at grain boundaries. This means that the dislocation density in Ti decreases initially. With a strain of 250, the $(10\bar{1}1)$ peak of Ti shifts

https://doi.org/10.1557/jmr.2014.18 Published online by Cambridge University Press

to a high angle for ~0.2°, and this indicates that a large amount of the Al has diffused into the Ti lattice. The higher Al content in the Ti lattice contributes to a lower dislocation velocity, and the pinning dislocations can interact and tangle with each other or newly formed dislocations may be generated. As a result, a very high density of dislocation is present in the Ti.

A comparison of the long times required when ball milling Ti/Al to produce TiAl, Ti_3Al, and $TiAl_3$, 80–100 h,[1] with our results suggests that the formation of intermetallic compounds is enhanced by the shear strain imposed during HPT, which facilitates diffusion. It is interesting to note that no intermetallic phases were detected in the ball milled Ti–Al system when processed by ECAP even at elevated temperatures up to 350 °C.[9] However, processing of pure Ti and Al sheets by friction stir welding was shown to result in the formation of $TiAl_3$.[30] In a recent study on coarse-grained Al–Cu (fcc/fcc) system processed by HPT, an enhanced diffusion and solid state reaction of aluminum and copper was reported, and the formation of intermetallic compounds such as Al_2Cu, AlCu, and Al_4Cu_9 was observed after 100 HPT revolutions.[11] The formation of intermetallic phases in HPT-deformed samples should be studied in the context of thermodynamics and the kinetics of diffusion. Thermodynamic calculations suggest that, in equilibrium conditions, the Ti and Al diffusion couple forms TiAl and $TiAl_3$ phases. By contrast, the formation of $TiAl_3$ and $TiAl_2$ phases was reported upon extrusion of elemental Ti and Al powder and subsequent reactive sintering.[31] The formation of Ti–Al intermetallics was previously reported in powder metallurgy of elemental Ti and Al and reaction synthesis of the mixture.[32] The free energy of formation of intermetallics in the Ti–Al system from the literature[33] is listed in Table II and the sequence of reactions between elemental Ti and Al may be described as

$$6\mathrm{Ti} + 6\mathrm{Al} \rightarrow 4\mathrm{Ti} + 2\mathrm{TiAl_3} \quad ,$$

$$4\mathrm{Ti} + 2\mathrm{TiAl_3} \rightarrow \mathrm{Ti_3Al} + \mathrm{TiAl} + 2\mathrm{TiAl_2} \quad .$$

The sequence of reactions and associated free energy of formation show that $TiAl_3$ is the first phase that forms during a reaction between elemental Ti and Al in the cryomilled sample subjected to HPT; $TiAl_2$ was subsequently formed via a reaction between Ti and $TiAl_3$, and this was confirmed by HRTEM as shown in Fig. 4. Since the formation of intermetallics typically requires elevated temperatures, it then becomes important to ascertain the influence of kinetics of the diffusion phenomena on the formation of intermetallics in the HPT-processed cryomilled powder. As discussed above, a fine nanostructure with a high density of dislocations is formed during cryomilling, as shown in Table I and Fig. 3. The grain boundaries and lattice defects (i.e., dislocations and vacancies) are possible short-circuits for diffusion of the Al into the Ti. In related studies, enhanced diffusion for solid state formation of intermetallics in a coarse-grained Al–Cu system processed by HPT was reported by Oh-ishi et al.[11] Diffusion calculations have shown that the kinetics of the diffusion in HPT-processed samples is comparable to surface diffusion rather than grain boundary and lattice diffusion. This fast diffusion was attributed to the availability of a high density of dislocations and a high concentration of vacancies and grain boundaries all formed during cryomilling.

Furthermore, the application of high pressure promotes diffusion by affecting the activation volume of diffusion. On the basis of thermodynamic considerations, the activation volume is related to pressure as[34]:

$$\Delta V = \left(\frac{\partial \Delta G}{\partial p}\right)_T \quad ,$$

where ΔG is the Gibbs free energy of diffusion:

$$\Delta G = G^{\mathrm{F}} + \mathrm{G}^{\mathrm{M}} \quad .$$

G^{F} and G^{M} are the free energy of formation and migration of defects, respectively, for the defect-mediated mechanism such as substitutional diffusion in the Ti–Al system. As discussed in more detail in the literature,[11] the pressure-assisted diffusion alone can elevate the diffusion coefficient to $10^{12}-10^{22}$ times higher than the lattice diffusion. This effect causes the coarse grain mixture of Al–Cu to form intermetallics after 100 HPT turns. In our system, the cryomilled material also has a reduced length scale, and therefore a decreased diffusion distance, due to the presence of nanostructures of Ti and Al. Furthermore, the cryomilled powder stored a high density of lattice defects that provide fast diffusion paths for atomic species.

The important role of shear strain in facilitating atomic movements has recently been the topic of various studies. Molecular dynamics studies of atomic mixing in fcc/fcc and fcc/bcc metals under shear deformation showed that, depending on the coherency of the interface, the atomic mixing can occur differently. For coherent interfaces, mixing occurs as dislocations transfer across phase boundaries. However, a diffusive mixing mechanism operates when shear strain is applied to an incoherent

TABLE II. Free energy of formation of intermetallic compounds in Ti–Al system.[33]

Compound	Free energy of formation at T = 340 K, ΔG_f (J/mol)
Ti_3Al	−27355
TiAl	−31733
$TiAl_3$	−36813
$TiAl_2$	−40118

https://doi.org/10.1557/jmr.2014.18 Published online by Cambridge University Press

interface, causing a local shuffling of atoms at the interface.[35] This is in agreement with the fast diffusion of atoms observed in severely deformed material in different systems such as Ni,[36] Cu–Pb,[37] Al–Mg, and Al–Zn.[38] Our observations in the Ti/Al system also confirm that in a hcp/fcc diffusion couple, the shortened diffusion distance and applied shear strain during HPT readily triggers the formation of intermetallic compounds. HPT deformation of a nanostructured Ti/Al mixture and the in situ formation of intermetallic compounds by shear strain-assisted diffusion facilitate the production of bulk nanostructured composite samples with intermetallic phases present. Elevated temperature HPT on coarse-grained powder has been used previously for producing intermetallic compounds from elemental powders in Ti–Al[6] and Ni–Al[5] systems. By using cryomilled powder as a precursor for the HPT processing, it is evident that the elevated temperature HPT is not required. This approach may also be useful for minimizing the adverse impact of the Kirkendall effect that leads to the formation of voids in diffusion couples of elements with significant differences in atomic size and diffusion coefficient.[39]

V. CONCLUSIONS

(1) A nanostructured Ti/Al mixture with a high dislocation density and grain sizes of 42 and 100 nm for the Al and Ti, respectively, was synthesized via cryomilling. The cryomilled powder was then used as a precursor for HPT processing.

(2) It was found that the reduced diffusion distance and availability of diffusion paths through grain boundaries, dislocations, and vacancies, together with an applied shear strain under high pressure during HPT processing, provide a pathway for the in situ solid state formation of intermetallic compounds (i.e., $TiAl_3$ and $TiAl_2$ in the Ti–Al system) at HPT strains as low as $\gamma = 22$ at ambient temperature.

(3) Further HPT deformation up to $\gamma = 98$ and 250 was found to contribute to microstructure refinement in both the titanium and aluminum metallic phases and intermetallics formed at $\gamma = 22$.

ACKNOWLEDGMENTS

Three of the authors (HB, YS, and EJL) acknowledge support from the National Science Foundation (Grant No. DMR-1210437) and General Motors Global R&D (Warren, MI). Two of the authors (JW-N and TGL) acknowledge support from the National Science Foundation under Grant No. DMR-1160966.

REFERENCES

1. M.R. Farhang, A.R. Kamali, and M. Nazarian-Samani: Effects of mechanical alloying on the characteristics of a nanocrystalline Ti-50 at.%Al during hot pressing consolidation. *Mater. Sci. Eng., B* **168**(1–3), 136 (2010).
2. A.P. Zhilyaev and T.G. Langdon: Using high-pressure torsion for metal processing: Fundamentals and applications. *Prog. Mater. Sci.* **53**(6), 893 (2008).
3. R.Z. Valiev and T.G. Langdon: Principles of equal-channel angular pressing as a processing tool for grain refinement. *Prog. Mater. Sci.* **51**(7), 881 (2006).
4. G. Angella, P. Bassani, A. Tuissi, and M. Vedani: Intermetallic particle evolution during ECAP processing of a 6082 alloy. *Mater. Trans.* **45**(7), 2182 (2004).
5. K. Edalati, S. Toh, M. Watanabe, and Z. Horita: In situ production of bulk intermetallic-based nanocomposites and nanostructured intermetallics by high-pressure torsion. *Scr. Mater.* **66**(6), 386 (2012).
6. K. Edalati, S. Toh, H. Iwaoka, M. Watanabe, Z. Horita, D. Kashioka, K. Kishida, and H. Inui: Ultrahigh strength and high plasticity in TiAl intermetallics with bimodal grain structure and nanotwins. *Scr. Mater.* **67**(10), 814 (2012).
7. Y. Li, Y.H. Zhao, W. Liu, C. Xu, Z. Horita, X.Z. Liao, Y.T. Zhu, T.G. Langdon, and E.J. Lavernia: Influence of grain size on the density of deformation twins in Cu–30%Zn alloy. *Mater. Sci. Eng., A* **527**(16–17), 3942 (2010).
8. J. Wongsa-Ngam, H. Wen, and T.G. Langdon: Microstructural evolution in a Cu–Zr alloy processed by a combination of ECAP and HPT. *Mater. Sci. Eng., A* **579**(0), 126 (2013).
9. E.W. Lui, W. Xu, X. Wu, and K. Xia: Multiscale two-phase Ti–Al with high strength and plasticity through consolidation of particles by severe plastic deformation. *Scr. Mater.* **65**(8), 711 (2011).
10. H. Bahmanpour, K.M. Youssef, J. Horky, D. Setman, M.A. Atwater, M.J. Zehetbauer, R.O. Scattergood, and C.C. Koch: Deformation twins and related softening behavior in nanocrystalline Cu-30% Zn alloy. *Acta Mater.* **60**(8), 3340 (2012).
11. K. Oh-ishi, K. Edalati, H.S. Kim, K. Hono, and Z. Horita: High-pressure torsion for enhanced atomic diffusion and promoting solid-state reactions in the aluminum–copper system. *Acta Mater.* **61**(9), 3482 (2013).
12. R.B. Figueiredo, P.R. Cetlin, and T.G. Langdon: Using finite element modeling to examine the flow processes in quasi-constrained high-pressure torsion. *Mater. Sci. Eng., A* **528**(28), 8198 (2011).
13. R.B. Figueiredo, P.H.R. Pereira, M.T.P. Aguilar, P.R. Cetlin, and T.G. Langdon: Using finite element modeling to examine the temperature distribution in quasi-constrained high-pressure torsion. *Acta Mater.* **60**(6–7), 3190 (2012).
14. B.D. Cullity: *Elements of X-Ray Diffraction*, 2nd ed. (Addison-Wesley Pub. Co., Reading, MA, 1978).
15. A.J.C. Wilson: *X-Ray Optics; The Diffraction of X-Rays by Finite and Imperfect Crystals* (Methuen, London, 1949).
16. G.K. Williamson and R.E. Smallman: Dislocation densities in some annealed and cold-worked metals from measurements on the X-ray Debye-Scherrer spectrum. *Philos. Mag.* **1**(1), 34 (1956).
17. O. Ertorer, T. Topping, Y. Li, W. Moss, and E.J. Lavernia: Enhanced tensile strength and high ductility in cryomilled commercially pure titanium. *Scr. Mater.* **60**(7), 586 (2009).
18. D.B. Witkin and E.J. Lavernia: Synthesis and mechanical behavior of nanostructured materials via cryomilling. *Prog. Mater. Sci.* **51**(1), 1 (2006).
19. M. Oehring, T. Klassen, and R. Bormann: The formation of metastable Ti-Al solid-solutions by mechanical alloying and ball-milling. *J. Mater. Res.* **8**(11), 2819 (1993).
20. S. Kumaran, T.S. Rao, R. Subramanian, and P. Angelo: Nanocrystalline and amorphous structure formation in Ti-Al system during high energy ball milling. *Powder Metall.* **48**(4), 354 (2005).
21. K. Edalati, Z. Horita, T. Furuta, and S. Kuramoto: Dynamic recrystallization and recovery during high-pressure torsion: Experimental evidence by torque measurement using ring specimens. *Mater. Sci. Eng., A* **559**(0), 506 (2013).

https://doi.org/10.1557/jmr.2014.18 Published online by Cambridge University Press

22. Y.B. Wang, J.C. Ho, Y. Cao, X.Z. Liao, H.Q. Li, Y.H. Zhao, E.J. Lavernia, S.P. Ringer, and Y.T. Zhu: Dislocation density evolution during high pressure torsion of a nanocrystalline Ni-Fe alloy. *Appl. Phys. Lett.* **94**(9), 091911 (2009).
23. L. Li, T. Ungár, Y.D. Wang, G.J. Fan, Y.L. Yang, N. Jia, Y. Ren, G. Tichy, J. Lendvai, H. Choo, and P.K. Liaw: Simultaneous reductions of dislocation and twin densities with grain growth during cold rolling in a nanocrystalline Ni–Fe alloy. *Scr. Mater.* **60**(5), 317 (2009).
24. X.Z. Liao, A.R. Kilmametov, R.Z. Valiev, H. Gao, X. Li, A.K. Mukherjee, J.F. Bingert, and Y.T. Zhu: High-pressure torsion-induced grain growth in electrodeposited nanocrystalline Ni. *Appl. Phys. Lett.* **88**(2), 021909 (2006).
25. Y. Qian, S. Zhi-Wei, L. Ju, H. Xiaoxu, X. Lin, S. Jun, and E. Ma: Strong crystal size effect on deformation twinning. *Nature* **463**(7279), 335 (2010).
26. C. Suryanarayana: Mechanical alloying and milling. *Prog. Mater. Sci.* **46**(1–2), 1 (2001).
27. R. Kirchheim: Reducing grain boundary, dislocation line and vacancy formation energies by solute segregation. I. Theoretical background. *Acta Mater.* **55**(15), 5129 (2007).
28. Y. Wang, D.J. Srolovitz, J.M. Rickman, and R. Lesar: Dislocation motion in the presence of diffusing solutes: A computer simulation study. *Acta Mater.* **48**(9), 2163 (2000).
29. S.Y. Hu, J. Choi, Y.L. Li, and L.Q. Chen: Dynamic drag of solute atmosphere on moving edge dislocations: Phase-field simulation. *J. Appl. Phys.* **96**(1), 229 (2004).
30. Y.C. Chen and K. Nakata: Microstructural characterization and mechanical properties in friction stir welding of aluminum and titanium dissimilar alloys. *Mater. Des.* **30**(3), 469 (2009).
31. G.X. Wang and M. Dahms: Synthesizing gamma-TiAl alloys by reactive powder processing. *JOM* **45**(5), 52 (1993).
32. G.X. Wang and M. Dahms: TiAl-based alloys prepared by elemental powder-metallurgy-overview. *Powder Metall. Int.* **24**(4), 219 (1992).
33. U.R. Kattner, J.C. Lin, and Y.A. Chang: Thermodynamic assessment and calculation of the Ti-Al system. *Metall. Trans. A* **23**(8), 2081 (1992).
34. H. Mehrer: *Diffusion in Solids: Fundamentals, Methods, Materials, Diffusion-controlled Processes* (Springer, Berlin, New York, 2007).
35. N.Q. Vo, J. Zhou, Y. Ashkenazy, D. Schwen, R.S. Averback, and P. Bellon: Atomic mixing in metals under shear deformation. *JOM* **65**(3), 382 (2013).
36. S.V. Divinski, G. Reglitz, H. Rösner, Y. Estrin, and G. Wilde: Ultra-fast diffusion channels in pure Ni severely deformed by equal-channel angular pressing. *Acta Mater.* **59**(5), 1974 (2011).
37. S.V. Divinski, J. Ribbe, D. Baither, G. Schmitz, G. Reglitz, H. Rösner, K. Sato, Y. Estrin, and G. Wilde: Nano- and micro-scale free volume in ultrafine grained Cu–1wt.%Pb alloy deformed by equal channel angular pressing. *Acta Mater.* **57**(19), 5706 (2009).
38. T. Fujita, Z. Horita, and T.G. Langdon: Using grain boundary engineering to evaluate the diffusion characteristics in ultrafine-grained Al–Mg and Al–Zn alloys. *Mater. Sci. Eng., A* **371**(1–2), 241 (2004).
39. H.N. Hersh: The Kirkendall effect in alloy systems. *J. Appl. Phys.* **23**(9), 1055 (1952).

https://doi.org/10.1557/jmr.2014.18 Published online by Cambridge University Press